IJMP

Original Article

Improvement of Breast Cancer Detection Using Non-subsampled Contourlet Transform and Super-Resolution Technique in Mammographic Images

Fatemeh Pak[1], Hamidreza Rashidy Kanan[1*]

Abstract

Introduction
Breast cancer is one of the most life-threatening conditions among women. Early detection of this disease is the only way to reduce the associated mortality rate. Mammography is a standard method for the early detection of breast cancer. Today, considering the importance of breast cancer detection, computer-aided detection techniques have been employed to increase the quality of mammographic images and help physicians reduce false positive rate (FPR).

Materials and Methods
In this study, a method was proposed for improving the quality of mammographic images to help radiologists establish a prompt and accurate diagnosis. The proposed approach included three major parts including pre-processing, feature extraction, and classification. In the pre-processing stage, the region of interest was determined and the image quality was improved by non-subsampled contourlet transform and super-resolution algorithm. In the feature extraction stage, some features of image components were extracted and skewness of each feature was calculated. Finally, a support vector machine was utilized to classify the features and determine the probability of benignity or malignancy of the disease.

Results
Based on the obtained results using Mammographic Image Analysis Society (MIAS) database, the mean accuracy was estimated at 87.26% and maximum accuracy was 96.29%. Also, the mean and minimum FPRs were estimated at 9.55% and 2.87%, respectively.

Conclusion
The results obtained using MIAS database indicated the superiority of the proposed method to other techniques. The reduced FPR in the proposed method was a significant finding in the present article.

Keywords: Breast Cancer, BI-RADS, Mammography, MIAS Database, Non-subsampled Contourlet Transform, Super Resolution, Support Vector Machine.

[1] *Department of Electrical, Computer and IT Engineering, Qazvin Branch, Islamic Azad University, Qazvin, Iran*
∗ Corresponding author: Tel: 09122454561; Email: h.rashidykanan@qiau.ac.ir

1. Introduction

Diagnosis of breast cancer is one of the most important issues in medical circles. Early detection of breast cancer can reduce the associated mortality rate and improve the survival of patients. Among all available methods, mammography is considered as the best technique for the early detection of this condition.

Two of the most prevalent symptoms of breast cancer are masses and calcifications. Diagnosis of breast cancer is normally difficult, considering the small size of some calcifications and the insignificant density difference between healthy tissues and masses. Therefore, given the importance of proper diagnosis, computer-aided detection (CAD) techniques have been employed in recent years to help physicians make a prompt and accurate diagnosis and reduce the false positive rate (FPR).

Timp and Karssemeijer developed CAD techniques to study interval changes between two consecutive mammographic screening rounds. They proposed methods for the detection of malignant masses, based on the features extracted from single mammographic views. They aimed to improve the detection process by including temporal information in CAD techniques. [1]

Moreover, Dominguez and Nandi improved mammographic images, based on statistical criteria. They segmented suspicious regions, using multi-level thresholding and extracted the features of different regions. Finally, a ranking system was employed in order to determine the suspicious regions. [2]

Meenalosini and Janet segmented the suspicious regions, using the region-growing method after removing noise from images; they extracted some features of tissues via spatial gray-level dependence. They used support vector machines for classifying the extracted features. [3]

Additionally, Oliver et al. segmented the region of interest (ROI) using a level-set algorithm, based on the region information.

They used Zernike moments to characterize each segmented mass for modelling its shape. Finally, Gentleboost algorithm was used for detecting the benignity or malignancy of the mass. [4]

In addition, Vadivel and Surendiran described each mass, using a shape feature vector, consisting of shape and margin properties. They used C5.0 decision tree algorithm to generate simple rules, which could be easily implemented and used in a fuzzy inference system. [5]

Furthermore, Rashed et al. performed a multi-resolution analysis of digital mammograms, using wavelet transform. They applied Euclidean distance to classify microcalcification clusters, normal mammograms, and speculated, circumscribed, or ill-defined masses. [6]

Among recently developed methods, wavelet transform is a well-known technique for the detection of breast lesions, Considering that lesions have high frequency components. [7-10]. However, despite the expanded application of this method, it has some limitations in capturing the directional information of images such as smooth contours and directional edges.

Contourlet transform (CT), which has been developed based on discrete wavelet transform, can be applied to eliminate the mentioned limitations. CT, first presented by Do and Vetterli, has other properties including directionality and anisotropy, in addition to the features of wavelet transform[11]. In this regard, Moayedi et al. used CT for extracting features from determined masses. [12]

However, since CT lacks shift invariance due to down-sampling and up-sampling, non-subsampled CT (NSCT) was proposed by Cunha et al. to compensate for this shortcoming [13]. Therefore, NSCT can be used in the proposed method in order to determine breast lesions according to their properties.

In this study, NSCT was applied for improving the quality of images after determining the

ROIs. Afterwards, super resolution (SR) algorithm was utilized to increase the resolution of images and the predicted high-frequency components; then, a high-pass filter was used to highlight the desired regions. In the next stage, image objects were obtained and 7 features (based on the shape, size, boundary, and density of breast lesions) were extracted; skewness of each feature was then calculated. Finally, the obtained feature matrix was provided for the support vector machine (SVM) algorithm to determine Breast Imaging-Reporting and Data System (BI-RADS).

2. Materials and Methods

The technique proposed in this study included 3 main stages: 1) pre-processing, 2) feature extraction, and 3) classification plus BI-RADS detection. Figure 1 shows the structure of the proposed method. In the following sections, we will describe each stage in detail.

2.1. Pre-processing

In order to obtain desirable results and distinguish between benign and malignant lesions, pre-processing was performed in two stages: ROI determination and quality improvement of mammographic images.

2.1.1. ROI detection

The first stage of pre-processing included the removal of additional margins, which minimizes images and reduces the computational burden (Figure 2b). On the other hand, some features of masses and calcifications are highly similar to tissue regions (e.g., pectoral muscles) or some artifacts (e.g., labels), which include the patient's information in the corner of images; these regions should be removed for reducing FPR to determine the ROI of mammographic images.

For this purpose, all images were aligned to the left side so that the pectoral muscle would be placed on the left side in all images; the images were labelled on the right side (Figure 2b). To remove the pectoral muscle and label from images, thresholding method and erosion morphological operator were utilized (Figure 2c).
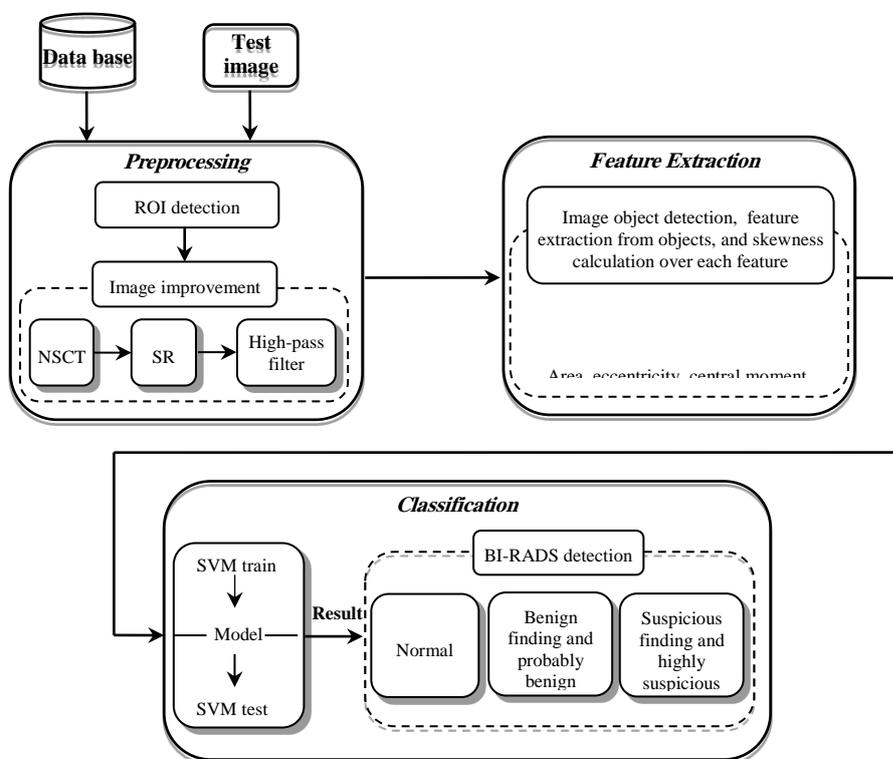

Figure 1. The structure of the proposed system

2.1.2. Improvement of mammographic images

It is necessary to promote the quality of mammographic images for highlighting masses and calcifications in breast tissues. In fact, image edges and regions can be effectively extracted and studied when the image quality is high. Since image edges are superposed with high-frequency components, a frequency-domain method should be applied. For this purpose, NSCT was applied in this study, and SR algorithm was utilized to increase the image resolution. Finally, a high-pass filter was used for sharpening and highlighting the desired regions.
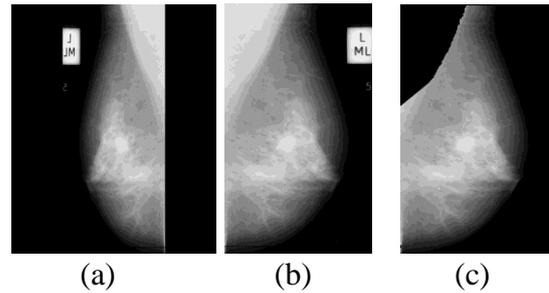

Figure 2. ROI detection: (a) the original image, (b) removal of additional margins and image alignment, (c) label and pectoral removal
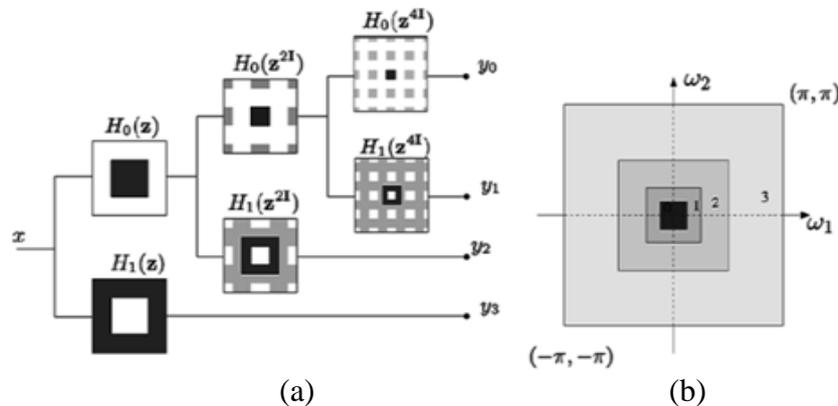

Figure 3. Non-subsampled pyramid: (a) three-stage pyramid decomposition (the lighter gray regions denote the aliasing caused by up-sampling), (b) subbands on the 2D frequency plane [13]

NSCT: In CT, a laplacian pyramid (LP) was first used to capture point discontinuities. Then, a directional filter bank (DFB) was employed to link point discontinuities into linear structures [11]. The final result was the expansion of the image, using basic elements including contour segments (called CT), which were implemented by a pyramidal DFB [11].

LP decomposition at each level generated a down-sampled low-pass version of the original image, indicating the difference between the original image and prediction results in a bandpass image. Due to down-sampling and up-sampling in both LP and DFB, CT was not shift-invariant. To achieve shift-invariant properties, NSCT was proposed by Cunha and colleagues [13]. NSCT is built upon non-subsampled laplacian pyramids (NSLP) (Figure 3) and non-subsampled DFB (NSDFB) (Figure 4) and is a fully shift-invariant, multi-scaled, and multi-directional decomposition.

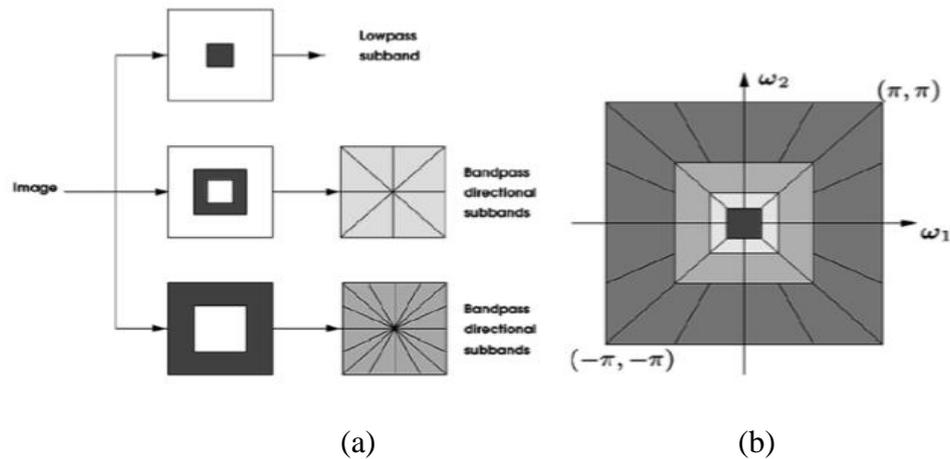(a)   (b)

Figure 4. NSCT: (a) NSDFB structure by implementing NSCT, (b) the idealized frequency partitioning obtained by the structure proposed by Cunha et al. [13]

SR algorithm: The goal of SR is to obtain a high-resolution image, based on one or a set of images with low resolution. Since SR technique is a way of increasing resolution without altering the existing imaging hardware, it can be suitable for medical imaging [14]. Overall, the objective of SR algorithm is to improve the resolution of images containing high-frequency components, in which aliasing and degradation have occurred. Therefore, SR can increase the sampling rate by utilizing the information of high-frequency components and reducing the aliasing effects, caused by the application of NSCT [14].

In general, SR techniques can be classified into four classes [15]: 1) a frequency-domain-based approach, 2) an interpolation-based approach, 3) a regularization-based approach, and 4) a learning-based approach. In the current study, SR technique, based on learning algorithms, was applied, given its suitability for overcoming single-image problems and its ability to predict high-frequency components.

1.   Improvement of the final image : In the proposed method, after determining the ROIs, image dimensions decreased to half of the main dimensions due to the large size of mammographic images and high computational rate. Then, three-level NSCT decomposition was applied and two subbands in the first level, four subbands in the second level, eight subbands in the third level, and one low-pass subband with low-frequency components were obtained.

Among the obtained subbands, only those with high-frequency components were used. To detect the image edges, Prewitt edge detector was used on each subband. In order to obtain the stronger edges of the image, standard deviation of each subband was calculated and considered as the threshold in Prewitt edge detector. After finding the edges in each subband, a weight was given to some regions of subbands (including the edges) to highlight the mentioned edges. Then, the image was reconstructed after changing its high-frequency subbands. The results of this stage are presented in Figure 5c.

In the proposed method, SR algorithm was used based on fuzzy learning algorithm after image reconstruction to improve image quality and increase its resolution (Figure 5d) [16]. Finally, a high-pass filter was used for sharpening and highlighting the desired regions. The final improved image is shown in Figure 5e.
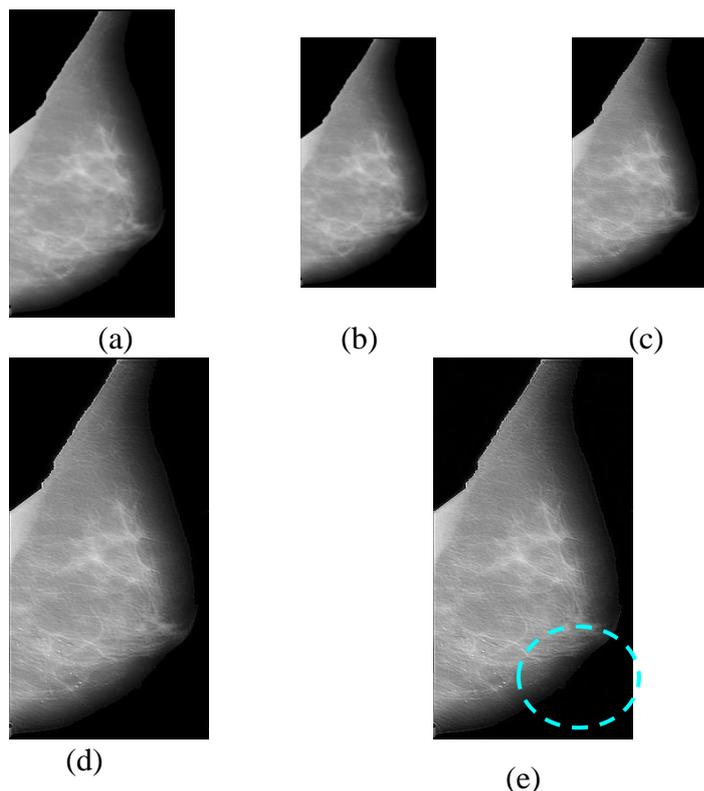
Figure 5. Image improvement steps: (a) the original image after ROI detection, (b) the resized image, (c) the improved image by applying NSCT, (d) the increased resolution of image (c) by applying fuzzy SR algorithm, (e) the final improved image by applying high-pass filter to image (d)

2.2. Feature extraction

In feature extraction stage, the information of mammographic images was extracted so that the system could accurately distinguish between normal and abnormal tissues. Since masses and calcifications have higher density and are brighter than other breast tissues, the histogram of improved images was obtained and the highest value (> 200) was selected to produce binary images including masses and calcifications. Then, regions available in images were labelled and objects of images were obtained.

At the end, some features including the shape, size, boundary, and density of breast lesions were extracted from image objects. Considering the importance of lesion shape in determination of lesion benignity or malignancy, features, which were related to the shape of lesions, were mostly considered in this study. These features included area [17, 18], eccentricity [17], central moment [17], fractal [18], spread [17], compactness [17, 18],

and the average gray level. These features are described below.

Area (A): This feature is suitable for describing the size of objects present in the image.

Eccentricity (E): It measures the degree to which an object's mass is concentrated along a particular axis, as defined in equation (1):

$$\varepsilon = \frac{(m_{2,0} - m_{0,2})^2 + 4m_{1,1}^2}{(m_{2,0} + m_{0,2})^2} \tag{1}$$

where for an image $f(x,y)$, the moment of order $p+q$ is defined as equation (2):

$$m_{pq} = \sum_x \sum_y x^p y^q f(x,y) \tag{2}$$

The range of values for this feature is 0-1. Values close to zero represent circular objects and values close to one indicate linear objects.

Central moment (M): This feature provides some information about the roughness of shapes. The central moment of order k in a distribution is defined as equation (3):

$$m_k = E(x - \mu)^k \tag{3}$$

where *E(X)* is the expected value of *X* and *k* is equal to four, since higher order moments are highly sensitive to noise [17]. The range of values for this feature is also 0-1. If this value is larger and close to one, irregularity occurs more frequently in shapes.

Fractal dimension (F): Micro-calcifications are small light local anomalies, which represent sharp local changes of contrast in the image from the fractal standpoint and are rare events in the global sense [19]. A higher fractal value corresponds to contour irregularity and thus a higher probability of malignancy.

Spread (S): This feature measures how unevenly objects are distributed around their centroid and is based on the central moments of boundary pixels. Spread is defined as equation (4):

$$S = \mu_{o,2} + \mu_{2,0} \tag{4}$$

where the moments *f(x,y)*, translated by an amount *(p, q)*, are defined as equation (5):

$$\mu_{pq} = \sum_x \sum_y (x - \bar{x})^p (y - \bar{y})^q f(x,y) \tag{5}$$

The range of values for this feature is also 0-1. Again, low values represent circular objects, while large values indicate linear and non-uniform objects.

Compactness (C): Compactness is a dimensionless quantity which provides a simple measure for complex counters. Compactness is independent of translation, rotation, and scale. This feature is defined as equation (6):

$$C = \frac{P^2}{4\pi A} \tag{6}$$

where *P* is the perimeter and *A* is the area of objects. The high value of this feature indicates an irregular and elongated object, while low values represent more symmetric and regular objects.

Average gray level (AG): Since masses and calcifications are brighter than their background, average pixel values of image objects can be considered as suitable features.

Considering the introduced features and their definitions, skewnessof each feature was calculated. Skewness (SK)is a measure of data asymmetry by which we can determine the

roughness or smoothness, regularity or irregularity, symmetry or asymmetry, circularity or linearity, and brightness of image objects and decide on their malignancy or benignity. Therefore, the feature vector was obtained for each image via equation (7):

$$F = [SK(A) \quad SK(E) \quad SK(M) \quad SK(F) \quad SK(S) \quad SK(C) \quad SK(AG)] \tag{7}$$

2.3. Classification and BI-RADS detection

In this study, multi-class SVM was used for the classification and determination of related BI-RADS [20]. Furthermore, k-nearest neighbour (KNN), naive bayes (NB), artificial neural network (ANN), and linear discriminant analysis (LDA) were used to compare the effectiveness of the proposed approach.

2.3.1. SVM

In general, it has been reported that the classification performance of SVM is superior to neural networks and other classification methods [20]; especially when the input data is too noisy, neural networks cannot provide reliable classification results. The formulation of SVMs embodies the structural risk minimization (SRM) principle.

In SVMs, the original input space is mapped onto a high-dimensional dot-product space via a kernel. The new space is called a feature space, in which an optimal hyperplane is determined to maximize the generalization ability. The optimal hyperplane can be determined by only few data points, called support vectors (SVs). Accordingly, an SVM can provide a good generalization performance for classification problems, despite the fact that it does not incorporate problem-domain knowledge; this attribute is unique to SVMs [20].

In the basic form, SVM learns the linear decision rule $f(x) = sign\{w\,x + b\}$, described by weight vector *w* and threshold *b*. Assuming that we have a data set as follows:

$$D = \{(x_i, y_i)\} \quad (i = 1, ..., l) \quad y_i \in \{-1, 1\} \tag{8}$$

where x_i is the input sample and y_i is the output class, y_i has two values (-1 or +1) that stand for two classes and *l* is the sample number. Therefore, the decision hyperplane can be expressed as equation (9):

$$w\,x + b = 0 \qquad (9)$$

If all the training data satisfy the constraints, then:

$$x_i\,w + b \geq +1 \quad for \quad y_i = +1, \quad \forall_i = 1,...,l$$
$$x_i\,w + b \leq -1 \quad for \quad y_i = -1, \quad \forall_i = 1,...,l \qquad (10)$$

The distance between the two hyperplanes is denoted by equation (11):

$$2d = \frac{2}{\|w\|} \qquad (11)$$

where distance d is considered as the safety margin of the classifier. The standard SVM model is:

$$\min_{w,b,\varepsilon_i} \quad J = \frac{1}{2}w^T w + C\sum_{i=1}^{l}\varepsilon_i ,$$
$$y_j(<w, x_i> +b) \geq 1 - \varepsilon_i ,$$
$$\varepsilon_i \geq 0, \quad i = 1,...,l \qquad (12)$$

where w is a vector of weights, b is a bias value, ε_i denotes the slack variable, and $< . , . >$ refers to an inner product. Its dual form is as follows:

$$\max \quad \sum_{i=1}^{l}\alpha_i - \frac{1}{2}\sum_{i=1}^{l}\sum_{j=1}^{l}\alpha_i\alpha_j y_i y_j <x_i, x_j>$$
$$\sum_{i=1}^{l} y_i\alpha_i = 0 \qquad (13)$$
$$0 \leq \alpha_i \leq C, i = 1,...,l$$

The abovementioned SVM is an essentially linear method, although it can be easily generalized to non-linear decision rules by replacing the inner products $<x_i, x_j>$ with a kernel function $K(x_i, x_j)$ [$K(x_i, x_j) = \varphi(x_i), \varphi(x_j)$] [21]. We only need to use K in the training algorithm and definition of φ is not required. The classifying function is shown in equation (14) [22].

$$f(x) = \sum_{i=1}^{l}\alpha_i y_i k(x_i, x_j) + b \qquad (14)$$

Some kernel functions [$K(x_i, y_j)$], proposed by Vapnik, are listed in Table 1. Polynomial and Gaussian functions are the most frequently used kernel functions. In this study, we used SVM-KM toolbox [23].

Table 1. Some investigated kernel functions for pattern-recognition problem [20]

Type of kernel	Kernel function
Polynomial of degree p	$K(x, y) = (x.y + 1)^p$
Gaussian radial basis function	$K(x, y) = e^{-\|x-y\|^2/2\sigma^2}$
Two-layer sigmoidal neural network	$K(x, y) = \tanh(kx.y - \delta)$

2.3.2. SVM-based multi-class classifier

There are two implementation algorithms for multi-class classification by SVM: "one against one" and "one against all". The "one-against-one" strategy, also known as "pair-wise coupling", "all pairs", or "round robin", consists of constructing one SVM for each pair of classes. Thus, for a problem with c classes, $c(c-1)/2$ SVMs are trained to distinguish the samples of one class from those of another class. An unknown pattern is usually classified according to maximum voting, where each SVM votes for one class.

The "one-against-all" strategy consists of constructing one SVM per class, which is trained to distinguish the samples of one class from those of all remaining classes. Normally, an unknown pattern is classified according to the maximum output among all SVMs.

These two algorithms generally provide satisfactory results. However, the choice of algorithm is of high significance for obtaining the optimal model, based on the problem under investigation. The number of classes and number of training samples for these strategies can be suitable parameters for solving the classification problem.

For problems with few classes, the "one-against-all" strategy seems significantly more accurate. On the other hand, for problems with a very large number of training samples, the training time can be problematic, and the "one-against-one" strategy appears more suitable for practical application [24]. Indeed, the "one-against-all" strategy is more accurate than "one against one". Thus, in this paper, we used this strategy for multi-class classification.

2.3.3. BI-RADS detection

The American College of Radiology (ACR) has classified mammographic images using BI-RADS in six general categories, based on breast lesions: [25]

1. BI-RADS 0: Incomplete evaluation
2. BI-RADS I: Normal
3. BI-RADS II: Benign finding
4. BI-RADS III: Probably benign
5. BI-RADS IV: Suspicious finding
6. BI-RADS V: Highly suspicious

In the proposed algorithm, based on the available information in the database, BI-RADS was determined in three classes: normal (BI-RADS I), benign (BI-RADS II, III), and malignant (BI-RADS IV, V).

3. Results

In this paper, Mammographic Image Analysis Society (MIAS) database was used to evaluate the effectiveness of the proposed method. This database includes 322 images (dimensions of 1024×1024) in seven groups, among which 208 images are normal and 80 images include masses and calcifications. Overall, 47 out of these 80 abnormal images show benign lesions, whereas 33 images indicate malignant lesions. [26]

It is necessary to mention that a set including 288 normal and abnormal images was used to test the proposed method. Table 2 shows the available information in the database for each mammogram.

In the proposed method, after determining the ROIs, three-level NSCT decomposition was applied for improving the quality of mammographic images; in each level, 2, 4, and 8 subbands were obtained, respectively. In image decomposition with NSCT, "maxflat" and "dmaxflat7" were used as NSLP and NSDFB filters, respectively. After improving the images and extracting the features of image objects, a feature matrix was allocated to SVM for determining BI-RADS. Experimental results indicate that when Gaussian kernel with a degree of 5 is used and the value of parameter C is equal to 10,000, the best results can be obtained.

To evaluate the proposed method, 16-fold cross validation was applied. In addition, to show the suitability of the proposed technique, some measures including sensitivity, specificity, accuracy, area under curve (AUC), F-measure, equal error rate (EER), and FPR were utilized. The equations of employed measures are demonstrated in Table 3.

Table 2. Mammogram information in MIAS database [26], Ex. mdb227 G CALC B 504 467 9

First column	Second column	Third column
Image name from MIAS database	Background tissue: F-fatty G-fatty-glandular D-dense-glandular	Class of abnormality: calcification (CALC), circumscribed masses (CIRC), spiculated masses (SPIC), ill-defined masses (MISC), architectural distortion (ARCH), asymmetry (ASYM), normal (NORM)
Fourth column	Fifth and sixth columns	Seventh column
Severity of abnormality: B (benign), M (malignant)	(x,y) image coordinates of the center of abnormality	Approximate radius (in pixel) of a circle enclosing the abnormality

Table 3. The employed measures for evaluating the proposed system

Measures	Equations
True positive rate (TPR)= sensitivity	$TP/P = TP/(TP+FN)$
True negative rate (TNR) = specificity	$TN/N = TN/(FP+TN)$
False negative rate (FNR) = 1-sensitivity	$FN/P = FN/(TP+FN)$
FPR = 1- specificity	$FP/N = FP/(FP+TN)$
Accuracy	$(TP+TN)/(TP+TN+FP+FN)$
AUC	$0.5*(Sensitivity+ Specificity)$
Precision	$TP/(TP+FP)$
Recall	$TP/(TP+FN)$
F-measure	$2 (Precision*Recall)/(Precision+Recall) = 2TP/(2TP+FN+FP)$
ERR	When FPR is equal to FNR

3.Results

For improving the quality of mammographic images and determining the edges of the image, NSCT was used as previously mentioned. Also, in order to investigate the capability of the proposed method, we compared NSCT with other frequency transforms such as CT and wavelet transform. Table 4 and Figure 6 [the detection error trade-off (DET) curves] indicate the effectiveness of our proposed algorithm. The highest mean accuracy, equal to 87.26%, was related to NSCT method with an FPR of 0.095, while CT and wavelet transform had lower accuracies and higher FPRs, compared to NSCT.
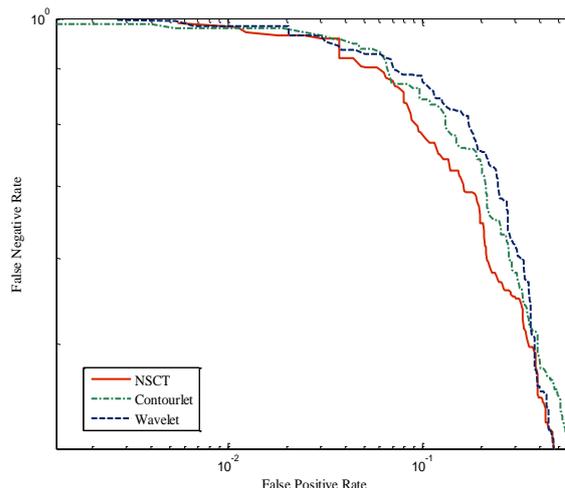

Figure 6. DET curves for the comparison of different time-frequency transforms

Table 4. Comparison of mammographic image improvement, using different time-frequency transforms

Methods	Mean accuracy	Mean AUC	Mean measure	F-	Mean EER	Mean FPR	Max accuracy
NSCT	87.26%	0.8567	80.90%		0.1432	0.0955	96.29%
CT	85.87%	0.8411	78.81%		0.1588	0.1059	92.59%
Wavelet transform	82.17%	0.7994	73.26%		0.2005	0.1337	96.29%

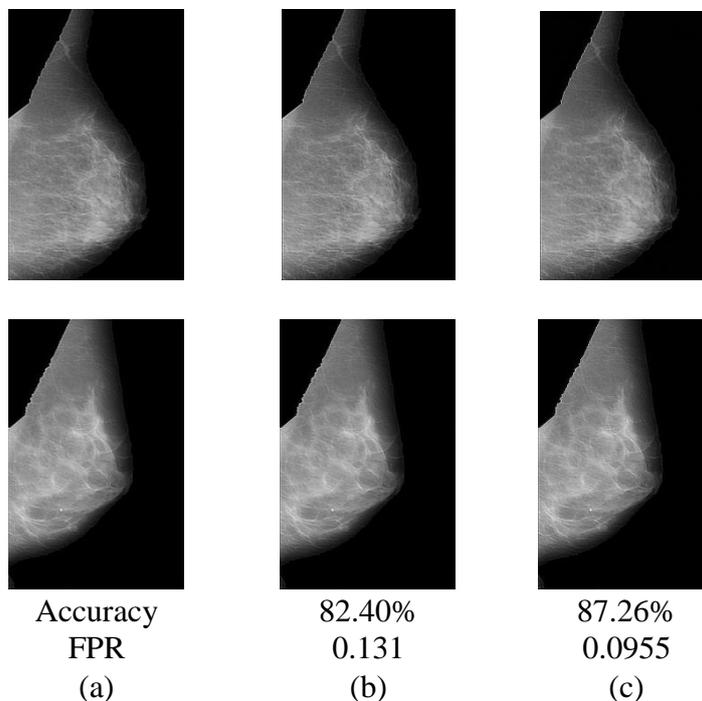|		
Accuracy	82.40%	87.26%
FPR	0.131	0.0955
(a)	(b)	(c)

Figure 7. Comparison of different SR methods: (a) the original image after applying NSCT, (b) application of SR algorithm based on bicubic interpolation, (c) applying SR algorithm based on fuzzy learning algorithm

In the second stage of image quality improvement, SR algorithm was used based on fuzzy algorithm. To indicate the superiority of the proposed algorithm, we compared it with

bicubic interpolation method, as shown in Figure 7. In the bicubic interpolation method, the mean accuracy was estimated at 82.40% and FPR was 0.131. Therefore, the accuracy was lower and the FPR was higher in the bicubic interpolation method, compared to the proposed SR technique.

Receiver operating characteristic (ROC) curves in Figure 8 show the performance of different kernel functions on MIAS database. As demonstrated in this diagram, the highest accuracy was obtained by using the Gaussian kernel. The parameters (type of kernel and the value of C parameter) were also tuned for grid search to improve the performance of the proposed approach.
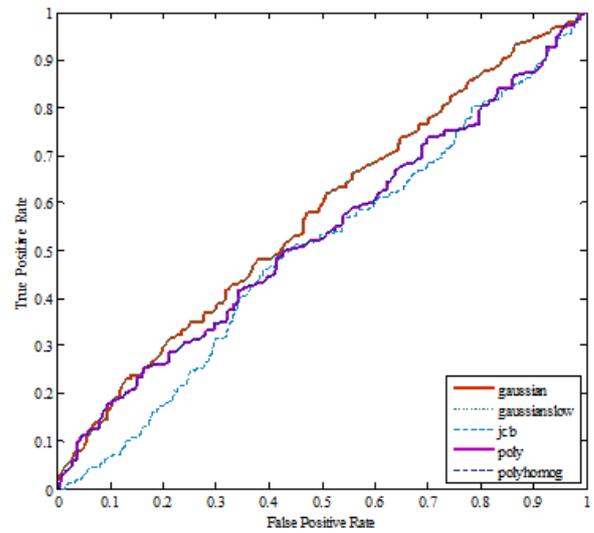

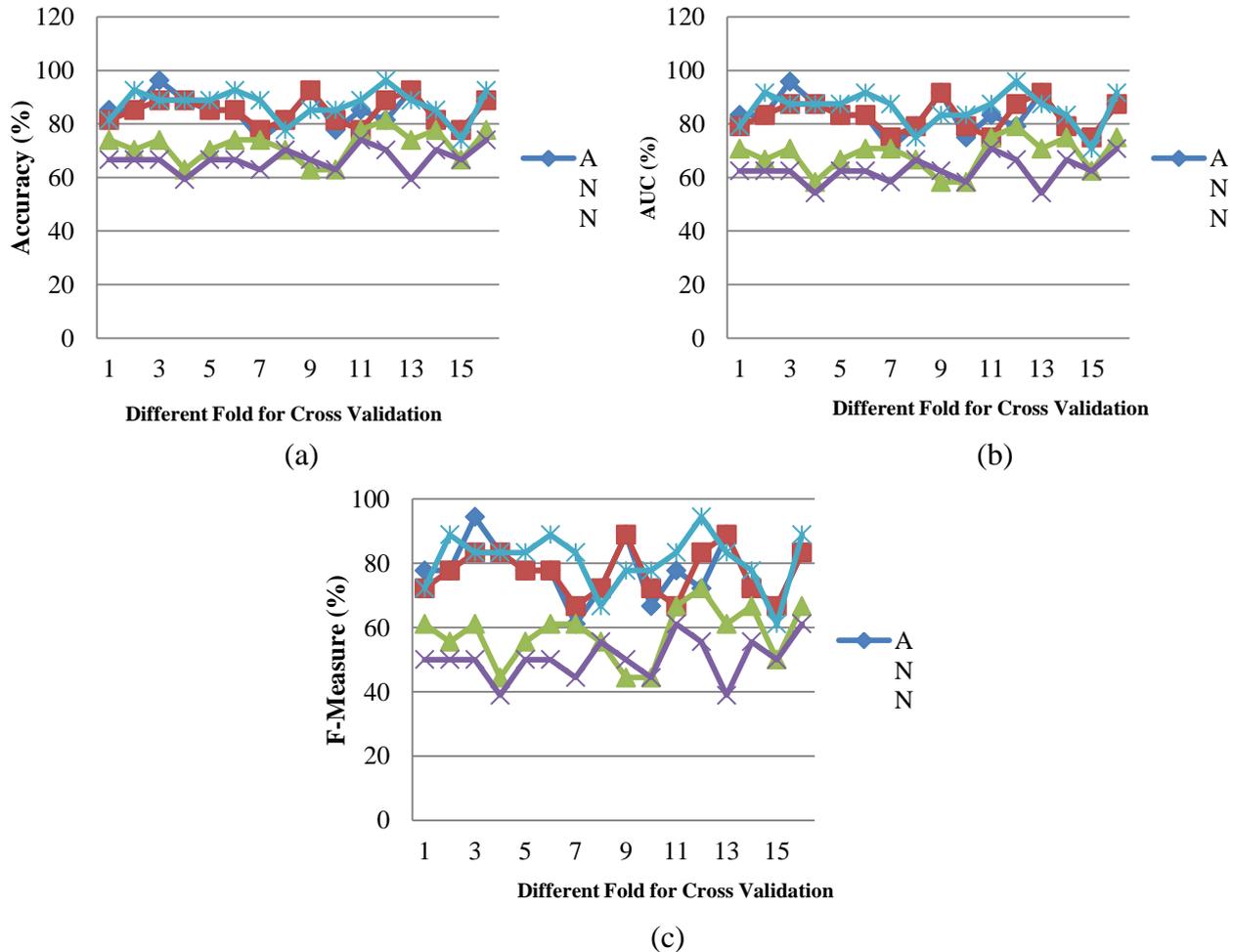Figure 8. Performance of different kernel functions on MIAS database

(a)

(b)

(c)

Figure 9. Comparison of different classifiers based on different measures: (a) based on accuracy (b) based on AUC, (c) based on F-measure.

To show the performance of the proposed classification, SVM results were compared with different methods, as presented in Figure 9. In this experiment, ANN, KNN, LDA, and NB classifiers were considered and compared with SVM. SVM showed the highest accuracy among other classifiers (Figure 9).

In the final experiment, to show the performance of the proposed technique, different folds were studied, as demonstrated in Figure 10; the best result was obtained using 16-fold cross validation. In Figure 10, the mean and maximum accuracies of different folds are presented.
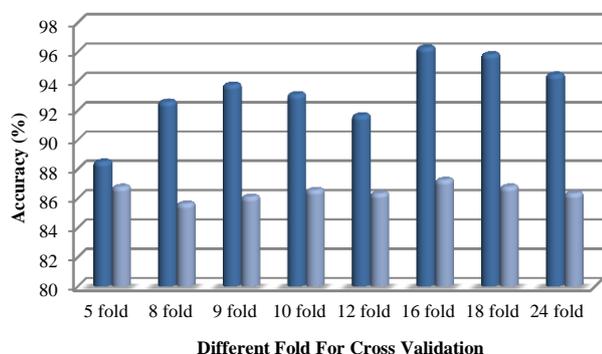

Figure 10. The accuracies obtained for a number of different folds. Dark blue: max accuracy, light blue: mean accuracy

4. Discussion

The goal of this study was to present a method for the early detection of breast cancer. Therefore, we attempted to improve the quality of mammographic images, increase their accuracy, and reduce the FPR. The obtained results showed the efficiency of this method, considering the maximum accuracy and minimum FPR (96.29% and 2.87%, respectively).

Indeed, the main contribution of the proposed method was the quality improvement of images and feature extraction. Therefore, we proposed an algorithm to compensate for limitations in previous methods. For this purpose, NSCT was used to detect high-frequency components that correspond to breast lesions after ROI detection to compensate for the limitations of other time frequencies such as wavelet transform and CT. Then, SR was used to increase the resolution of images and better predict high-frequency components. Afterwards, some features based on shape, size, boundary, and density of breast lesions were extracted and analysed by calculating skewness. We tried to include more features, compared to previously mentioned methods. Finally, SVM classifier as a good learning algorithm was used to determine BI-RADS.

Table 5 shows the results of comparison between the proposed method and other techniques, which have been tested on MIAS database. It should be noted that the maximum accuracy obtained for each method was noted. Therefore, the obtained results indicated the high performance of the presented method.

Table 5. Comparison of the proposed method with other techniques

Methods	Accuracy	Sensitivity	Specificity
Ferreira and Borges [8]	94.85%	--	--
Mohanalin et al. [27]	--	0.9375	--
Moayedi et al. [12]	82.1%	--	--
Meenalosini and Janet [3]	--	0.952	0.944
The proposed method (mean accuracy)	87.26%	0.8090	0.9045
The proposed method (max accuracy)	96.29%	0.9444	0.9722

5. Conclusion

In this paper, a method was presented for improving the quality of mammographic images and reducing FPR to help radiologists diagnose benign and malignant breast lesions more accurately and promptly. The presented

algorithm included 3 major parts: pre-processing, feature extraction, and classification. This method had different advantages. Firstly, NSCT was used unlike previous methods, which used wavelet transform for determining the edges of images; NSCT is preferred over other methods in frequency domain. Secondly, SR algorithm was used to better predict high-frequency components and remove distortions. Also, to obtain a system which can distinguish between normal and abnormal tissues, 7 features were extracted from the objects in mammographic images. Each feature was analysed by calculating its skewness to decide if it is malignant or benign. Experimental results showed that the proposed method had mean and maximum accuracy of 87.26% and 96.29%, respectively, based on cross-validation strategy on MIAS database. Overall, better results were obtained, compared to state-of-the-art approaches. Also, FPR of radiologists, which was equal to 15% in mammographic images, was reduced to 9.55% on average (maximum of 2.87%).

References

1. Timp S., Karssemeijer N. Interval change analysis to improve computer aided detection in mammography. Medical Image Analysis. 2006 February;1o(1):82-95.
2. Dominguez A., Nandi A. Detection of masses in mammograms via statistically based enhancement, multilevel-thresholding segmentation, and region selection. Journal of Computerized Medical Imaging and Graphics. 2008 June;32(4):304-315.
3. Meenalosini S., Janet J. Computer Aided Diagnosis of Malignancy in Mammograms. Eropean Journal of Scientific Research. 2012;72(3):360-368.
4. Oliver A., Torrent A., Liado X., Marti J. Automatic diagnosis of masses by using level set segmentation and shape description. International Conference on Pattern Recognition, 2010. P.2528-2531.
5. Vadivel A., Surendiran B. A fuzzy rule-based approach for characterization of mammogram masses into BI-RADS shape categories. Computer in Biology and Medicine. 2013 May;43(4):259-267.
6. Rashed E. A., Ismail I. A., Zaki S. I. Multiresolution mammogram analysis in multilevel decomposition. Pattern Recognition Letters. 2007 January;28(2):286–292.
7. Bozek J., Mustra M., Delac K., Grgic M. A Survey of Image Processing Algorithms in Digital Mammography. Advances in Multimedia Signal Processing and Communication. 2009;231:631-657.
8. Ferreira C. B. R., Borges D. L. Analysis of mammogram classification using a wavelet transform decomposition. Pattern Recognition Letters. 2003 April;24(7):973-982.
9. Sung-Nien Y., Kuan-Yuei L., Yu-Kun H. Detection of microcalcifications in digital mammograms using wavelet filter and Markov random field model. Computerized Medical Imaging and Graphics. 2006 April;30(3):163-173.
10. Alarcon-Aquino V., Starostenko O., Ramirez-Cortes J. M., Rosas-Romero R., Rodriguez-Asomoza J., Paz-Luna O. J., Vazquez-Munoz K. Detection of Microcalcification in Digital Mammograms Using the Dual-Tree Complex Wavelet Transform. Engineering Intelligent Systems.2009 March;17(1):49-63.
11. Do M. N., Vetterli M. The contourlet transform: an efficient directional multiresolution image representation. IEEE transactions on image processing : a publication of the IEEE Signal Processing Society. 2005;14(12):2091-2106.
12. Moayedi F., Azimifar Z., Boostani R., Katebi S. Contourlet-based mammography mass classification using the SVM family. Journal of Computers in Biology and Medicine. 2010 April;40(4):373-383.
13. Cunha A. L., Zhou J., Do M. N. The Nonsubsampled Contourlet Transform: Theory, Design, and Applications. IEEE Transaction On Image Processing. 2006 october;15(10):3089-3101.
14. Greenspan H. Super-Resolution in Medical Imaging. Published by Oxford University Press on behalf of the British Computer Society. 2008 January;52(1):43-63.
15. Tian J., Ma K. K. A survey on super-resolution imaging. Signal, Image and Video Processing. 2011 February;5(3):329-342.
16. Purkait P., Chanda B. Fuzzy-Rule Based Approach forSingle Frame Super Resolution. IEEE Inetrnational Conference on Fuzzy Systems. 2013. p.1-7.

17. Tembey M. Computer-aided diagnosis for mammographic microcalcification clusters. M.S.C.S. Thesis. University of South Florida. 2003.
18. Street W. N., Wolberg W. H., Mangasarian O. L. Nuclear Feature Extraction For Breast Tumor Diagnosis. International Symposium on Electronic Imaging: Science and Technology. 1993;1905:861-870.
19. Patel B. C., Sinha G. Early Detection of Breast Cancer using Self Similar Fractal Method. International Journal of Computer Applications. 2010 November;10(4):39-43.
20. Burges C. J. C. A tutorial on Support Vector Machines for pattern recognition. Data Mining and Knowledge Discovery.1998 June;2(2):121-167.
21. Zhou Q., Hong W., Shao G., Cai W. A New SVM-RFE Approach towards Ranking Problem. IEEE Proc. Intelligent Computing and Intelligent Systems. 2009. p.270-273.
22. Benzerrouk A., Morello B. C., Zerhouni N. Evoling class for SVM's incremental learning. 16th International Conference on Computing in section Artificial Intelligence and Applications, Mexico City:Mexique. 2007.
23. Canu S., Grandvalet Y., Guigue V., Rakotomamonjy A. SVM and Kernel Methods Matlab Toolbox. 2005.
24. Milgram J., Cheriet M., Sabourin R. "One Against One" or "One Against All":Which One is Better for Handwriting Recognition with SVMs?. Tenth International Workshop on Frontiers in Handwriting Recognition. October 2006.
25. Giannakopoulou G., Spyrou G. M., Antaraki A., Andreadis L., Koulocheri D., Zagouri F., Nonni A., Filippakis G. M., Nikita K. S., Ligomenides P. A., Zografos G. C. Downgrading BIRADS 3 to BIRADS 2 category using a computer-aided microcalcification analysis and risk assessment system for early breast cancer. Journal of Computer in biology and Medicine. 2010 November-December;40(11-12):853-859.
26. MIAS database, http://peipa.essex.ac.uk/info/mias.html, Access time. 6 February 2015.
27. Mohanalin, Beenamol, Kalra P. K., Kumar N. A novel automatic microcalcification detection technique using Tsallis entropy & a type II fuzzy index. Journal of Computers and Mathematics with Applications. 2010 October;60(8):2426-2432.